Nonlinear Dyn (2010) 60: 217–229
DOI 10.1007/s11071-009-9591-z

ORIGINAL PAPER

Predicting the coefficient of restitution of impacting elastic-perfectly plastic spheres

Robert L. Jackson · Itzhak Green · Dan B. Marghitu

Received: 15 September 2008 / Accepted: 2 September 2009 / Published online: 27 September 2009

Abstract The current work presents a different methodology for modeling the impact between elasto-plastic spheres. Recent finite element results modeling the static deformation of an elasto-plastic sphere are used in conjunction with equations for the variation of kinetic energy to obtain predictions for the coefficient of restitution. A model is also needed to predict the residual deformation of the sphere during rebound, or unloading, of which several are available and compared in this work. The model predicts that a significant amount of energy will be dissipated in the form of plastic deformation such that as the speed at initial impact increases, the coefficient of restitution decreases. This work also derives a new equation for the initial critical speed which causes initial plastic deformation in the sphere that is different than that shown in previously derived equations and is strongly dependant on Poisson's Ratio. For impacts occurring above this speed, the coefficient of restitution will be less than a value of one. This work also compares the predictions between several models that make significantly different predictions. The results of the current model also compare well with some existing experimental data. Empirical fits to the results are provided for use as a tool to predict the coefficient of restitution.

Keywords Nonlinear force · Contact force · Impact · Elasto-plastic deformation · Coefficient of restitution

R.L. Jackson (✉) · D.B. Marghitu
Department of Mechanical Engineering, Auburn University, Auburn, AL 36849, USA
e-mail: robert.jackson@eng.auburn.edu

I. Green
Woodruff School of Mechanical Engineering, Georgia Institute of Technology, Atlanta, GA 30332, USA
e-mail: itzhak.green@me.gatech.edu

Nomenclature

A	area of contact
B	contact area material property coefficient
C	critical yield stress coefficient
E	elastic modulus
H_G	hardness geometric limit
K	hardness factor
m	mass
P	contact force
U_c	strain energy to cause initial plastic deformation
R	radius of hemispherical asperity
S_y	yield strength
V	velocities at initiation and end of contact
W	work
a	contact radius
e	coefficient of restitution
t	time
v	instantaneous velocities during contact
z	dummy variable having a direction normal to the impact surface

ε_y yield strength to elastic modulus ratio, S_y/E
η Poisson's ratio
ρ density
ω interference between hemisphere and surface

Subscripts
1 initial value just before impact
2 value just after impact
c critical value at onset of plastic deformation
e elastic regime
ep elasto-plastic regime
m maximum
res residual (after unloading from plastic deformation)

Superscripts
‘ equivalent
$*$ normalized by critical value

1 Introduction

The impact of spheres has many applications to objects of similar geometries, such as in shot peening [1, 2], impacts in sports [3, 4], projectile impacts [5, 6], and many others. It also has application in the contact of rough surfaces which is often modeled by a collection of spherical surface asperities [7, 8]. Some cases which may make use of a rough surface elasto-plastic impact model are electro-magnetic read-write heads [9–11], mechanical seals [12], rolling element bearings [13], and in electronics reliability [14, 15]. In read-write heads and mechanical seals, the hydrodynamic lubricating film which normally separates the surfaces may be intermittently broken when impulse loads cause surface contact to occur.

In these applications, the spherical contact model can be incorporated into frameworks for rough surface contact (statistical, fractal, and multiscale methods). Then the single impact model can be used to predict the impact between many small asperities or bumps on a surface, which are often idealized as spheres. This is especially useful for mechanical components that undergo periodic starts and stops that result in surfaces impacting. For instance, in read-write heads the nanoscale lubricating film will be compromised when the sliding motion of the head is stopped, and the film will also be compromised by the intermittent contacting of asperities that are taller than the lubricating film.

Several past works have used a simplified approach to modeling the plastic deformation of impacting spheres [16], such as the Chang, Etsion, and Bogy (CEB) model [7, 17]. The current work builds on these models by employing the recent results of an extensive finite element model of elasto-plastic spherical contact [18]. The results will allow for the prediction of the coefficient of restitution between two impacting elasto-plastic spheres (neglecting friction and other sources of energy dissipation).

The effect of elastic waves propagating away from the contact is neglected in the current work, however, Yang and Komvopolous [19] have investigated the elastic waves propagating from contact between a rigid sphere and an elastic half space. From their analysis, it appears that this effect is most important during the initial contact of the spheres (when deformations are small). In contrast, the current work analyzes the case of significantly larger deformations that involve plasticity. However, both of these mechanisms will probably simultaneously influence the coefficient of restitution of impacting spheres.

Chang and Ling [7] derived an equation for the coefficient of restitution using the CEB model [17]:

$$e^2 = \left\{ \frac{8}{15} E' \sqrt{R} \left[\omega_c \omega_m \left(2 - \frac{\omega_c}{\omega_m} \right) \right]^{3/2} \right\} \Bigg/ \left\{ \frac{8}{15} E' \sqrt{R} (\omega_c)^{5.2} + \pi (1.282 + 1.158\upsilon) S_y R \omega_m (\omega_m - \omega_c) \right\} \tag{1}$$

Thornton [20] derived a closed form equation to model the coefficient of restitution by dividing the problem into a perfectly elastic portion and perfectly plastic portion. The resulting equation is

$$e = 1.442 \left(1 - \frac{1}{6} \left(\frac{V_c}{V_1} \right)^2 \right)^{1/2} \times \left(\frac{\frac{V_c}{V_1}}{\frac{V_c}{V_1} + 2[\frac{6-(V_c/V_1)^2}{5}]^{1/2}} \right)^{1/4} \tag{2}$$

Using the finite element method, Wu et al. [21] also investigated the impact of spherical objects, but provided equations only for “finite plastic deformation.” An accompanying work by Li et al. [22] provides a theoretical model for lower velocities, but does not provide a closed form model. Finally, Weir and Tallon

[23] also derive an equation to predict the coefficient of restitution:

$$e = 3.1\left(\frac{S_y}{E'}\right)^{5/8}\left(\frac{R_1}{R}\right)^{3/8}\left(\sqrt{\frac{E'}{\rho}}\frac{1}{V_1}\right)^{1/4} \tag{3}$$

In addition, when $R_1 = R$ (as is the current case), (3) reduces to the simplified impact model given by Johnson [24].

Vu-Quoc and Zhang [25] also analyze the elasto-plastic contact of spheres. They use finite element results to find the force displacement curves to evaluate the coefficient of restitution. However, final closed-form equations are not provided and comparison with the current work results is not readily feasible. Nevertheless, they compare their results to Thornton [20]. Their results suggest that (2) under predicts the coefficients of restitution. This is consistent with the findings of the current work.

The current study employs the Hertz solution [26] to model elastic contact and the recent model of Jackson and Green [18] to model elasto-plastic contact (JG). This work assumes the material to behave as elastic-perfectly plastic and so is focused on the impact of ductile metallic materials.

2 Methodology

2.1 Elastic contact model

First, the static contact models employed in this work are summarized. The Hertzian solution [26] provides closed-form expressions to the deformations and stresses of two spheres in a purely elastic contact. For this case, no energy is lost to plastic deformation. If Hertz contact is used solely in predicting the coefficient of restitution, then the value of one unit should result. The two spheres may have different radii and different elastic properties. However, the closed-form solution renders an equivalent case where a single elastic sphere, having an equivalent elastic modulus, E', and an equivalent radius, R, is in contact with a rigid flat (see Fig. 1). The interference, ω, can be described as the distance the sphere is displaced normally into the rigid flat. The equations for elastic Hertz contact are well known and readily available in the literature.

2.2 Spherical elastic-perfectly plastic contact model

As the load or interference increases, the stresses within the hemisphere also increase. These stresses eventually cause the material within the sphere to yield. The interference at this initial point of yielding is known as the critical interference, ω_c. The recent work by Jackson and Green [18] derives this critical interference analytically using the von Mises yield criterion. Although previous works have derived the critical values as a function of hardness [17, 27], Jackson and Green [18] provide them as a function of yield strength since the relationship between hardness and yield strength has proven not to be constant. The resulting equation is

$$\omega_c = \left(\frac{\pi \cdot C S_y}{2E'}\right)^2 R \tag{4}$$

where C is

$$C = 1.295\exp(0.736\eta) \tag{5}$$

The values of Poisson's ratio, η, and yield strength, S_y, to be used in (5) are those of the material that yields first. To determine which material yields, one has to use the combination of CS_y, such that $CS_y = \min(C(\eta_1)S_{y1}, C(\eta_2)S_{y2})$, accounts for the

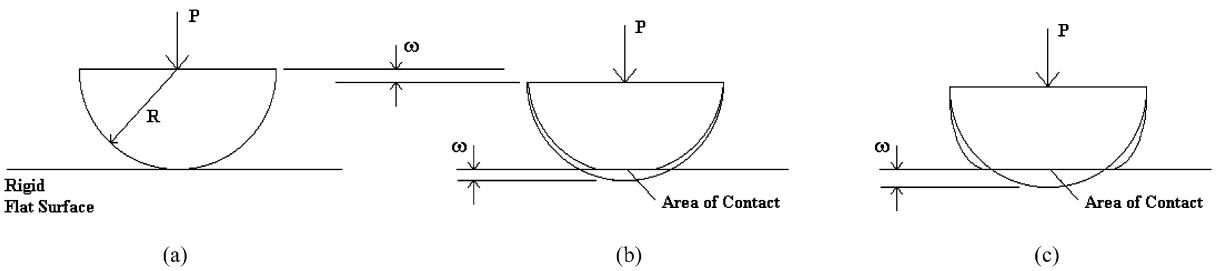

Fig. 1 Spherical contact model before contact (**a**), during mostly elastic deformation (**b**), and during mostly plastic deformation (**c**)

possibility of two different material properties (see [28]).

The critical force or load, P_c, is then calculated from the critical interference, ω_c, by substituting it into Hertz theory. The resulting critical contact force at initial yielding is

$$P_c = \frac{4}{3}\left(\frac{R}{E'}\right)^2\left(\frac{\pi}{2}CS_y\right)^3 \tag{6}$$

Similarly, the critical contact area is given by

$$A_c = \pi^3\left(\frac{CS_yR}{2E'}\right)^2 \tag{7}$$

The JG model predicts the contact force and area between an elastic perfectly plastic hemisphere and a flat. At $0 \le \omega/\omega_c \le 1.9$ the JG single asperity model effectively coincides with the Hertzian solution (the Hertz solution for elastic contact is then used), even though the onset of plastic deformation occurs at $\omega/\omega_c = 1$. At interferences (ω/ω_c) larger than 1.9, the formulation below is used as the current point contact model for modeling elasto-plastic impact:

For $\omega \ge 1.9 \cdot \omega_c$

$$A_{ep} = \pi R\omega\left(\frac{\omega}{1.9\omega_c}\right)^B, \tag{8}$$

$$P_{ep} = P_c\left\{\left[\exp\left(-\frac{1}{4}\left(\frac{\omega}{\omega_c}\right)^{\frac{5}{12}}\right)\right]\left(\frac{\omega}{\omega_c}\right)^{3/2} + \frac{4H_G}{CS_y}\left[1-\exp\left(-\frac{1}{25}\left(\frac{\omega}{\omega_c}\right)^{\frac{5}{9}}\right)\right]\frac{\omega}{\omega_c}\right\} \tag{9}$$

where

$$B = 0.14\exp(23\cdot\varepsilon_y), \tag{10}$$

$$\varepsilon_y = \frac{S_y}{E'}, \tag{11}$$

$$\frac{H_G}{S_y} = 2.84 - 0.92\left(1-\cos\left(\pi\frac{a}{R}\right)\right) \tag{12}$$

Quicksall et al. [29] confirmed these results for a wider range of materials by varying E, S_y and η. Equation (12) is a more concise version of a similar expression given in [18] that is valid for $0 < a/R < 1$. The predictions of the above equations also compare well with the few experimental results available [30, 31].

In order to further generalize the results of the current work, the critical values defined in (4–7) are used to normalize the results of all the models. This normalization scheme has been employed in many previous works [8, 17, 18, 27, 32]. The normalized parameters are

$$\omega^* = \omega/\omega_c, \tag{13}$$

$$P_e^* = P_e/P_c = (\omega^*)^{3/2}, \tag{14}$$

$$A_e^* = A_e/A_c = \omega^* \tag{15}$$

The elasto-plastic relationships (8–12) can also be normalized in the same way.

2.3 Coefficient of restitution

The traditional coefficient of restitution for normal contact of a ball against a rigid flat is defined as the ratio of the magnitudes of the relative velocities just after to just before impact:

$$e = \left|\frac{V_2}{V_1}\right| \tag{16}$$

where V_1 is the magnitude of the relative velocity before impact and V_2 is the magnitude of the relative velocity after impact. Please note that uppercase V denotes initial and final velocities at the center of the sphere, while the lowercase v symbols that follow shall denote instantaneous or intermediate velocities also at the center of the sphere.

For a perfectly elastic impact, when no energy is transferred to plasticity, friction, or elastic waves, $e = 1$. Therefore, this case is trivial. Once the load increases enough to cause yielding of the material, the problem is no longer trivial. This is the elasto-plastic case considered in the current work. The motion of the center of the sphere during the collision can then be specified by one of the following three phases: The first phase is elastic, meaning the loads are not great enough to cause plastic deformation. Once the load and resulting stresses are large enough to cause plastic deformation, the elasto-plastic phase is researched until the maximum load is reached. Finally, once the sphere begins to unload, the final phase of restitution begins until the surfaces are no longer in contact. These phases will be described in more detail in the following sections.

2.4 Phase I. Elastic compression phase

This phase starts with the contact instant ($P = 0$) and ends when the contact force reaches the known value of the critical force ($P = P_c$). For the critical force the deformation is the critical deformation ($\omega = \omega_c$). During this phase, there are only elastic deformations ($\omega < \omega_c$) and the Hertz model is applied.

Then the variation of the kinetic energy is

$$\frac{1}{2}m(v)^2 - \frac{1}{2}m(V_1)^2 = -\int_0^{\omega} (P_e)\, dz \tag{17}$$

where z is a dummy variable representing the intermediate interference (ω in (8, 9, 13–15)) when ω is the interference at the instant when the instantaneous velocity is v. The right-hand side of (17) is negative because the velocity and force are in opposite directions (this same convention is used in the remainder of this work). Then substituting in the contact force from the Hertz model results in

$$\frac{1}{2}m(v)^2 - \frac{1}{2}m(V_1)^2 = -\frac{4}{3}E'\sqrt{R}\int_0^{\omega} (z^{3/2})\, dz \tag{18}$$

and then integrating

$$\frac{1}{2}m(v)^2 - \frac{1}{2}m(V_1)^2 = -\frac{8}{15}E'\sqrt{R}\omega^{5/2} \tag{19}$$

Then rearranging

$$v = \sqrt{V_1^2 - \frac{16}{15}\frac{E'}{m}\sqrt{R}\omega^{5/2}} \tag{20}$$

This phase will end when plastic deformation begins, at $\omega = \omega_c$. Substituting $\omega = \omega_c$ into (20) provides a prediction for the critical velocity at which the sphere will begin to yield plastically according to the von Mises yield criteria:

$$v_c = \sqrt{V_1^2 - \frac{16}{15}\frac{E'}{m}\sqrt{R}\omega_c^{5/2}} \tag{21}$$

This critical velocity, v_c, is the instantaneous velocity during impact at which the sphere begins to deform plastically (which is also the end of Phase I).

2.5 Phase II. Elasto-plastic compression phase

The plastic deformations will appear in the second stage when the contact force is greater than the critical force, P_c. In this range, the current work will explore the use of several different elasto-plastic contact models. First, the elasto-plastic spherical contact JG model will be used (see (8–12)). The model by Chang and Ling [7], which is based on the popular CEB model [17] are also compared to the current results.

Using the JG Model, the equations do not simplify in a closed-form and, therefore, are solved numerically. For this phase, a normalized version of the variation in kinetic energy is used:

$$(W_{ep})^* = \frac{W_{ep}}{U_c} = \frac{1}{U_c}\left[-\int_{\omega_c}^{\omega} P_{ep}\, dz\right] \tag{22}$$

where $W_{ep} = \frac{1}{2}m(v)^2 - \frac{1}{2}m(v_c)^2$ and U_c is the maximum strain energy that the sphere can accumulate before deforming plastically. From Green [28], it is given as

$$U_c = \frac{(\pi \cdot C S_y)^5 R^3}{60E'^4} \tag{23}$$

and if (23) is written in terms of (4) and (6), then

$$U_c = \frac{2}{5}P_c\omega_c \tag{24}$$

Then (22) can be nondimensionalized as

$$(W_{ep})^* = \frac{W_{ep}}{U_c} = \frac{5}{2P_c\omega_c}\left[-\int_{\omega_c}^{\omega} P_{ep}\, dz\right] = -\frac{5}{2}\int_1^{\omega^*} P_{ep}^*\, dz^* \tag{25}$$

Substituting in (8–12) and numerically integrating (25) results in the relations shown in Fig. 2. These results use the properties shown in Table 1. All results shown in this work will use the properties in Table 1 unless noted otherwise. The total variation in kinetic energy is then

$$\frac{1}{2}m(v)^2 - \frac{1}{2}m(V_1)^2 = W_{ep} - \frac{8}{15}E'\sqrt{R}\omega_c^{5/2} \tag{26}$$

V_c is now defined as the critical initial velocity. When the $V_1 < V_c$ the impact is elastic, but when $V_1 \geq V_c$ then impact is considered elasto-plastic. V_c can be derived from

$$\frac{1}{2}m(V_c)^2 = \int_0^{\omega_c} (P_e)\, d\omega = U_c \tag{27}$$

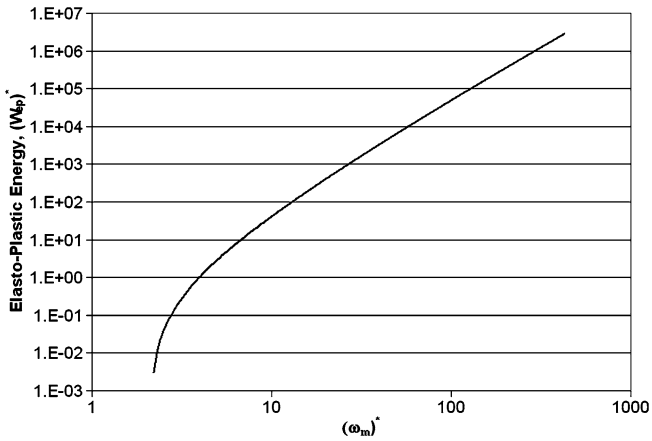

Fig. 2 Normalized elasto-plastic energy as a function of the normalized maximum interference

Table 1 Material properties and input parameters used as the benchmark case in the current analysis

E	200 GPa
S_y	1.12 GPa
η	0.33
R	0.01 m
c	1.651
ε_y	0.005
ω_c	1.335 μm
P_c	51.8 N
m	0.0327 kg

Substituting in the Hertz model for elastic contact into (27), integrating and solving for V_c results in

$$V_c = \sqrt{\frac{4\omega_c P_c}{5m}} = \sqrt{\frac{2U_c}{m}} \tag{28}$$

V_c provides the initial velocity before impact that will result in an impact that deforms the sphere plastically. This is to not be confused with v_c given in (21) for the instantaneous velocity at which the sphere starts deforming plastically during impact. Relating these equations, when $V_1 = V_c$ then by definition $v_c = 0$. Also, when $V_1 < V_c$ the impact is elastic and $e = 1$. Alternatives for (28) are given by Johnson [24], Thornton [20], and Wu et al. [33], however, these previous equations neglect the effect that Poisson's ratio has on the initiation of yielding (taken into account in the current work by the value C as defined by (5)). Algebraically the ratios between the previous equations and (28) can easily be derived where

$$V_c/(V_y)_{\text{Johnson}} = \sqrt{\frac{(\pi \cdot C)^5}{3180}},$$

$$V_c/(V_y)_{\text{Thornton}} = \sqrt{C^5},$$

and

$$V_c/(V_y)_{\text{Wu\_et\_al.}} = \sqrt{\left(\frac{C}{1.6}\right)^5}.$$

For a typical range of Poisson's ratios, η, these ratios are calculated and compared in Table 2. Clearly the prediction by Thornton [20] differs significantly from all the others. Evaluating the differences between the remaining equations, for $\eta = 0.3$, these equations show differences of 3% or less, while substituting in other typical values for Poisson's ratio results in differences as large as nearly 50%. Even for $\eta = 0.4$ the difference is 23.6% when comparing (28) to Johnson's version and 23.0% when it is compared to Wu et al. version. Therefore, the Poisson's ratio has an important effect in the calculation of the critical velocity, as incorporated in (28).

Then the maximum deflection, ω_m, can be found as a function of V_1, by setting $v = 0$ in (26) such that

$$\frac{1}{2}m(V_1)^2 = -\int_{\omega_c}^{\omega_m} P_{ep}\, dz - \frac{8}{15}E'\sqrt{R}\omega_c^{5/2} \tag{29}$$

which is solved to provide ω_m as a function of V_1, shown in Fig. 3, where V_1 is normalized by

$$(V_1)^* = \frac{V_1}{V_c} \tag{30}$$

Table 2 Comparison between (28) and previous critical velocity predictions as a function of Poisson's ratio η

η	0.1	0.15	0.2	0.25	0.3	0.35	0.4	0.45	0.5
C	1.394	1.446	1.500	1.557	1.615	1.675	1.738	1.803	1.871
$V_c/(V_y)_{\text{Johnson}}$	0.712	0.780	0.855	0.938	1.028	1.127	1.236	1.355	1.486
$V_c/(V_y)_{\text{Wu\_et\_al.}}$	0.708	0.777	0.852	0.934	1.024	1.122	1.230	1.349	1.479
$V_c/(V_y)_{\text{Thornton}}$	2.294	2.515	2.757	3.023	3.314	3.634	3.984	4.368	4.789

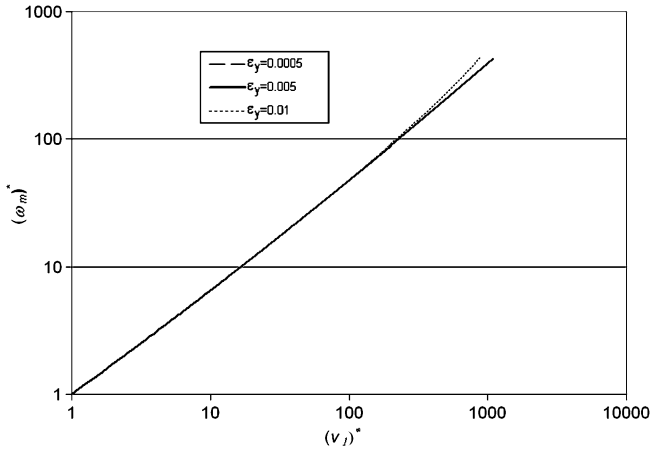

Fig. 3 Normalized maximum interference as a function of the normalized initial velocity

and ω_m is normalized such that

$$(\omega_m)^* = \frac{\omega_m}{\omega_c} \tag{31}$$

As expected, $(\omega_m)^*$ increases with $(V_1)^*$ (see Fig. 3). It should be noted that the relationship between $(\omega_m)^*$ and $(V_1)^*$ varies only slightly with ε_y.

2.6 Phase III. Restitution phase

The last phase is the restitution phase. The contact force decreases from the maximum value, P_m, to zero. Since $(\omega_m)^*$ is now known as a function of $(V_1)^*$, it is possible to calculate the restitution phase or elastic rebound of the sphere using the JG model. It is assumed that the sphere recovers in a completely elastic manner then the Hertz solution can be used to model the contact force as the sphere rebounds. The sphere will not fully recover to its original shape so the radius of curvature will change to R_{res} and the surface will be compressed permanently by a residual interference, ω_{res}. Then this elastic force of restitution will start by equaling the elasto-plastic force at $\omega = \omega_m$ such that

$$(P_{ep})_m = \frac{4}{3}E'\sqrt{R_{res}}(\omega_m - \omega_{res})^{3/2} \tag{32}$$

There are two ways by which R_{res} and ω_{res} can be obtained. First, from Etsion et al. [34],

$$\frac{\omega_{res}}{\omega_m} = 1 - \frac{3(P_{ep})_m}{4E'a_m\omega_m}, \tag{33}$$

$$R_{res} = \frac{4E'(a_m)^3}{3(P_{ep})_m} \tag{34}$$

where a_m is the contact radius at the maximum interference, ω_m. The second way is by fitting an equation to the finite element results of Jackson, Chusoipin, and Green [35].

$$\frac{\omega_{res}}{\omega_m} = 1.02\left(1 - \left(\frac{(\omega^*)_m + 5.9}{6.9}\right)^{-0.54}\right) \tag{35}$$

This fit is shown in Fig. 4 alongside the numerical data of [35]. Also, since (32) must always be satisfied, R_{res} is solved for as

$$R_{res} = \frac{1}{(\omega_m - \omega_{res})^3}\left(\frac{3}{4}\frac{(P_{ep})_m}{E'}\right)^2 \tag{36}$$

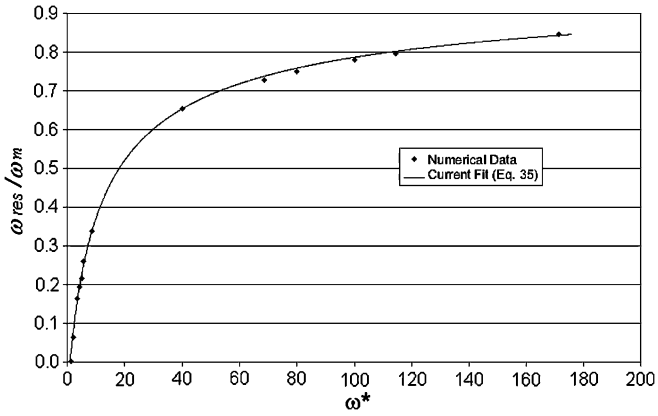

Fig. 4 Plot of new fit of the residual interference data provided by [35]

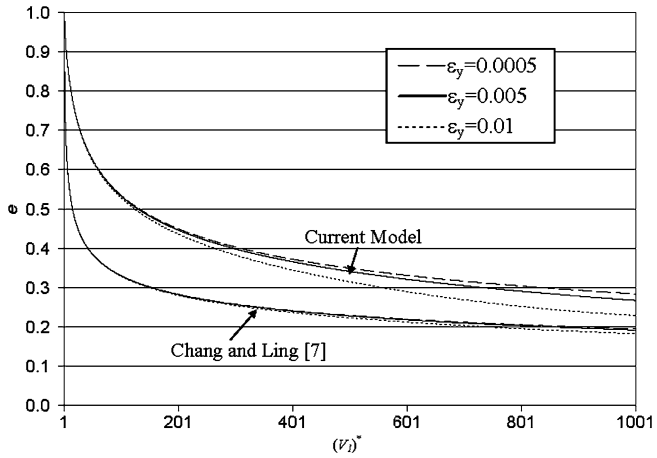

Fig. 5 Comparison of coefficient of restitution for different ε_y values as a function of normalized velocity for the current model and the CL model (based on CEB model)

Then the final velocity of the sphere as it comes out of contact with the flat is solved from

$$\frac{1}{2}m(V_2)^2 = \int_{\omega_m-\omega_{res}}^{0}\left(\frac{4}{3}E'\sqrt{R_{res}}(z)^{3/2}\right)dz \qquad (37)$$

giving

$$V_2 = \sqrt{\frac{16E'}{15m}}(R_{res})^{1/4}(\omega_m-\omega_{res})^{5/4} \qquad (38)$$

Here, either (33) or (35) can be used to solve for ω_{res}.

3 Results

To solve for the coefficient of restitution, (29) is first numerically integrated. Then the result of the integration and (33) or (35) is substituted into (38). Finally, the prediction for V_2 is substituted into (16). The coefficient of restitution, e, can then be obtained as a function of the $(V_1)^*$, and is plotted in Figs. 5 and 6. The effect of varying material and geometrical properties such as the yield strength, elastic modulus, Poisson's ratio, and sphere radius are also explored. Again, each parameter is varied from the benchmark case given by Table 1. By varying the elastic modulus and yield strength independently, it is found that the effect of each variable is the exact inverse of the other. In Fig. 5, the effects of these two variables can be quantified by observing the effect of the single combined variable, $\varepsilon_y = S_y/E'$. As expected, the normalization of V_1 by V_c succeeds in shifting the location of each curve to coincide at $e = 1$ for all material properties. Another trend that emerges from this is that as ε_y is increased, the magnitude of the slope decreases. It was also found that the radius does not affect the trends in this normalized form. The current analysis also considers the effect of Poisson's ratio over the range $0.2 < \eta < 0.45$. Although not shown the results show that Poisson's ratio, η, alone only has a minor effect on the predicted normalized results.

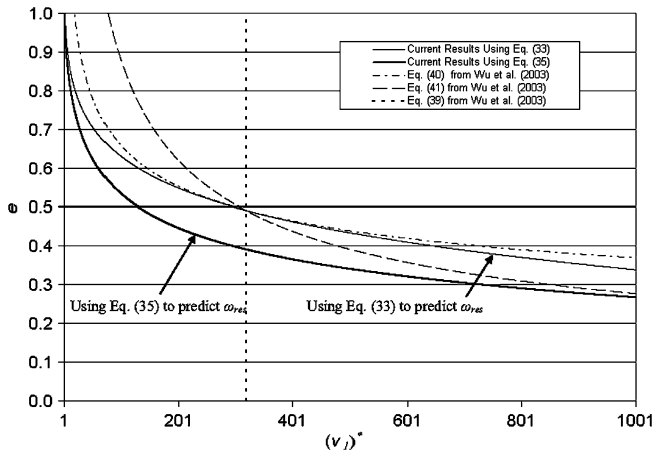

Fig. 6 The effect of the residual interference model on the predicted coefficient of restitution

3.1 Effect of residual interference equation

As discussed previously, the residual interference can be calculated by either (33) or (35). Figure 6 shows how these two equations affect the calculation of e as a function of $(V_1)^*$. It is observed that while the qualitative trends of e when using of (33) and (35) to calculate the residual interference are very similar, they noticeably differ quantitatively where (33) results in a higher prediction of e. The results shown are also compared to the model by Wu et al. [33] which is discussed in the following section.

3.2 Comparison to previous models and experimental results

In this section, the model outlined above is compared to the Chang and Ling (CL) model [7] which is based on the well-known CEB elasto-plastic spherical contact model [17]. See Fig. 5 for a comparison of these two models. Clearly, the two different models give very different predictions. The CL model also changes fairly little from variations in yield strength, ε_y, and it predicts a lower e than the current model. Interestingly, the current model and the CL model appear to approach each other at higher values of $(V_1)^*$. This agrees with intuition because the CL model predicts the contact to become fully plastic immediately after initial yielding (thus predicting low e values), in contrast to the current model which includes smoother transitions from elastic to elasto-plastic and eventually fully plastic deformation. Eventually, the CL model approaches the current model as plastic deformation increases. However, there are still other differences since the current model predicts that hardness will decrease with deformation.

Wu et al. [33] also provide a prediction of the coefficient of restitution based on finite element modeling. Wu et al. define a critical velocity, V_{fp}, above which the contact is considered to be undergoing "finite-plastic-deformation." According to Wu et al. [33],

$$V_{fp} = 0.008 \cdot V_c \cdot \left(\frac{E'}{S_y}\right)^2 \tag{39}$$

For $V_1 < V_{fp}$, the coefficient of restitution is predicted by

$$e = 2.08 \cdot \left(\frac{V_1}{V_c}\right)^{-1/4} \tag{40}$$

while for $V_1 > V_{fp}$ another equation is suggested

$$e = 0.62 \cdot \left(\frac{V_1}{V_c}\frac{S_y}{E'}\right)^{-1/2} \tag{41}$$

For the material properties considered herein, the threshold defined by V_{fp} is calculated and is shown by the vertical line in Fig. 6. It is seen that for $V_1 < V_{fp}$ the equations provided by Wu at al. [33] over-predict the coefficient of restitution in comparison to the current results. Moreover, (40 and 41) both forecast unrealistic values ($e > 1$, or $e \gg 1$, respectively) as V_1 approaches V_c. In the vicinity of $V_1 = V_{fp}$, (40) tends to agree with the current results when (33) is used to predict the force-displacement relationship during recovery but diverges outside of this region, while for $V_1 \gg V_{fp}$ (41) tends to approach the current results when (35) is used.

Table 3 Material properties used for modeling aluminum and aluminum oxide impact

E (aluminum)	68 GPa[a]
E (aluminum oxide)	370 GPa[a]
η (aluminum)	0.33[a]
η (aluminum oxide)	0.22[a]
S_y (aluminum)	0.38 GPa[b]
R	0.0025 m
c	1.651
ε_y	0.006
ω_c	0.474 μm
P_c	1.56 N
ρ (aluminum)	2700 kg/m^3[a]

[a]From Matweb.com

[b]From hardness given in [36]

Table 4 Material properties used for modeling steel and aluminum oxide impact

E (steel)	200 GPa[a]
E (aluminum oxide)	370 GPa[a]
η (steel)	0.29[a]
η (aluminum oxide)	0.22[a]
S_y (steel)	1.03 GPa[b]
R	0.0025 m
c	1.603
ε_y	0.0074
ω_c	0.721 μm
P_c	6.24 N
ρ (steel)	7800 kg/m^3[a]

[a]From Matweb.com

[b]From hardness given in [36]

The current model is now compared not only to the closed form models provided by Thornton [20], Wu et al. [33] and Weir and Tallon [23] but also to experimental results (see Figs. 7 and 8). It should be noted that now the velocities are not normalized by the critical velocity in these graphs as is done for previous graphs. Because the graphs are not normalized, the curves for the predicted coefficient of restitutions do not approach a value of unity at the same location. In addition, it is apparent that the critical velocity predicted by the Weir and Tallon [23] is much different than that predicted by the current methodology.

A comparison is done against the experimental results provided by Kharaz and Gorham [36]. For aluminum oxide spheres impacting an aluminum flat, the data is shown in Fig. 7, while for aluminum oxide spheres impacting a steel flat the data is shown in Fig. 8. In these experiments, the aluminum oxide spheres were believed to only deform elastically, such that the plastic deformation only occurred in the aluminum and steel flats. To compare these experimental results with the current model, the material properties in Tables 3 and 4 are used. The predictions of the current model, while using (35) to predict the residual interference in the sequence to calculate e, compares very well with the aluminum experimental results as shown in Fig. 7. Likewise, the results of using (35) to predict the residual interference also compare very well for the steel experiments (see Fig. 8) for $V < 0.5$ m/s, but do not compare as well past that range. Here, the incorporation of (33) in the current model compares better with the steel experimental results. Since it is suggested that strain hardening does occur in Kharaz and Gorham [36], these differences could be attributed to the fact that steel typically has a considerable strain hardening ratio (ultimate strength/yield strength) compared to aluminum. Since strain hardening is not considered in the current analysis, then aluminum experimental results are indeed projected to match better with the current model. Of course, the amount of strain hardening will be affected by the specific alloy of interest. For instance, the hardening tangent modulus of aluminum ranges from roughly 0.01 to 0.1 of the elastic modulus. At a value of 0.1, the hardening might be important, while at 0.01 it probably is not [37]. However, other recent studies [27, 37] find that strain hardening is not always a significant effect in spherical contact, especially at low impact velocities or load. The reason is that in typical spherical contact and impact the volume of plastic deformation and strain is relatively small, however, as the load is increased to induce more plastic deformation this might not be the case.

Other factors that could impact the results include strain rate dependant strength, elastic wave propagation, surface roughness, and the flat not being a true half space, and rotation of the sphere before and after impact; in addition to affecting the results, these factors could cause disagreement between the models and the experimental data. Regardless, the qualitative comparisons between the current models and the experimental results are by and large satisfactory and the

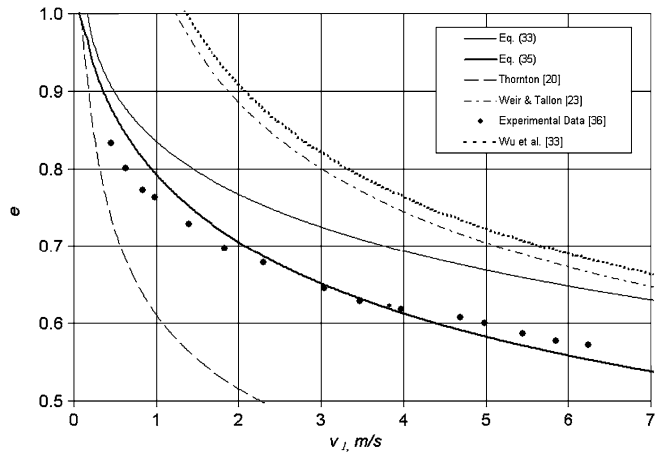

Fig. 7 Comparison of several models to experimental results aluminum oxide spheres impacting an aluminum flat

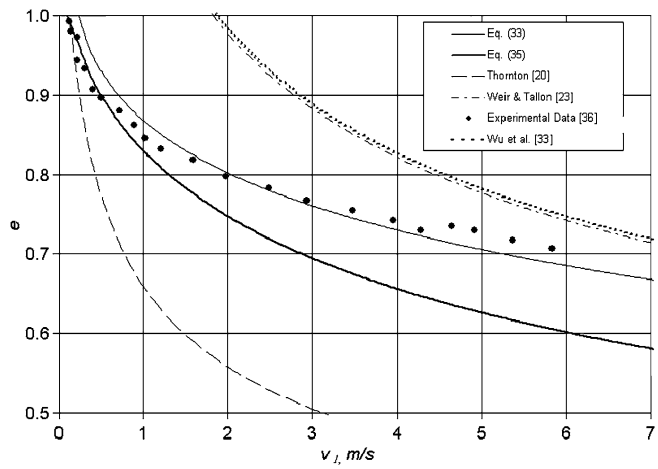

Fig. 8 Comparison of several models to experimental results aluminum oxide spheres impacting a steel flat

quantitative differences are also relatively minor. Likewise, it appears that the current model compares better with the experimental results than other recent models by Thornton [20] and Weir and Tallon [23]. As noted in Wu et al. [33], (40) is only valid for initial velocities that are 100 times greater than the initial critical velocity to cause yielding. This also means that this equation is not expected to compare well with the experimental results of [35] because they are for much lower velocities (see Figs. 7 and 8).

Another possible reason for the differences between the numerical and experimental results is the well-documented existence of strain rate dependant strength [38]. The strain rate effect usually increases the yield strength for metallic materials which should also result in higher predictions for the coefficient of restitution [39]. Since the local strain rate at any instant in the sphere is dependant on position and time, it is prohibitively difficult to accurately incorporate these results into the current methodology. A full finite element simulation which includes the strain gradient effects is probably needed for this purpose. However, it has been shown that aluminum is relatively unaffected by strain rates in comparison to steel [38]. This reinforces the agreement with the current comparison between the numerical and experimental results where the results for aluminum agree better than the results for steel. It is possible that by accurately including the strain rate effects in the current methodology the numerical and experimental results for steel will also be in closer agreement since the strain rate effect should increase the coefficient of restitution.

It is concluded that the current model predicts the coefficient of restitution reasonably well for both materials, but it still requires a numerical solution. Hence, empirical formulae may offer useful tools for engineering purposes.

3.3 Empirical equations

Two sets of empirical equations are fit to the results presented in this paper (one set for results using (33) to predict the residual interference and one set for (35)). When (35) is used to predict the residual interference in the sequence to predict e, a good fit resulted from the following set of equations:

For $0 < (V_1)^* < 1$

$$e = 1 \tag{42}$$

For $1 < (V_1)^* \leq 60$

$$e = 1 - 0.1\ln(V_1^*)\left(\frac{V_1^* - 1}{59}\right)^{0.156} \tag{43}$$

For $60 \leq (V_1)^* \leq 1000$

$$e = 1 - 0.1\ln(60) - 0.11\ln\left(\frac{V_1^*}{60}\right)(V_1^* - 60)^{2.36\varepsilon_y} \tag{44}$$

These equations combine to create a continuous prediction of e in the range of $0 < (V_1)^* < 1000$. Equations (42–44) differ from the current results shown in Fig. 5 by an average of 1.5% and by a maximum of 4.5%. When (33) is used to predict the residual interference in the sequence to predict e, a good fit results from the following equation:

For $1 < (V_1)^*$

$$e = 1 - 0.0361(\varepsilon_y)^{-0.114}\ln(V_1^*)(V_1^* - 1)^{9.5\varepsilon_y} \tag{45}$$

Equation (45) differs from the current results using (33) by an average of 5.3% and by a maximum of 8.4%. Equations (42–45) may not be valid outside the range specified in this work being $0.0005 < \varepsilon_y < 0.01$ and $0.2 < \eta < 0.45$.

The finite element model results used in the current work account for large deformations. The current calculations were limited to deformations up to about $(\omega_m)^* = 425$, which is within the range considered by the previous FEM investigation. Therefore, above that the model might not be as valid.

4 Conclusions

The current work sets forth a methodology for predicting the effect of elasto-plastic contact mechanics on the coefficient of restitution for an impacting sphere. The current work is successful at finding expressions for a critical velocity which causes the impacting sphere to deform plastically. These are different from those given by previous works that either neglect the effect of Poisson's ratio or are dependant on the hardness that is known to vary with other material properties and with the deformation itself. This work uses recent findings that depend solely upon indisputable material properties (E, S_y, and η). The said critical velocity is useful in normalizing the results for different materials. The current work also shows that the ratio of the yield strength to the elastic modulus, ε_y is the most influential variable in predicting the coefficient of restitution, once the initial velocity is normalized by the critical initial velocity. Different elasto-plastic contact models for loading [17, 18] and unloading [34, 35] are considered. Each of these different models appears to have a noteworthy effect on the predicted values for the coefficient of restitution.

The results are also compared to several existing theoretical models and experimental results. The current results compare well with the experimental results. Since other existing theoretical models do not compare as well, empirical equations are fitted to the current results to provide tools to predict the coefficient of restitution between impacting metallic spheres and surfaces. It should be noted that other researchers have suggested that strain hardening is the reason their models predict different results than what is seen in experiment. While the current results appear to partially agree with a recent analysis by Kogut and Etsion [27], which suggests that strain hardening actually plays a minor role, this and other works find that the strain rate (time) effect does appear to be meaningful.

References

1. Diepart, C.P.: Modelling of shot peening residual stresses—practical applications. Mater. Sci. Forum **163-6**(2), 457–464 (1994)
2. Eltobgy, M.S., Ng, E., Elbestawi, M.A.: Three-dimensional elastoplastic finite element model for residual stresses in the shot peening process. Proc. Inst. Mech. Eng., B J. Eng. Manuf. **218**(11), 1471–1481 (2004)
3. Peikenkamp, K.: Modelling of processes of impact in sports. J. Biomech. **22**(10), 1069 (1989)
4. Bowen, C.: Shaping the future of sports equipment. Mater. World **12**(5), 24–26 (2004)
5. Yasaka, T., Hanada, T., Hirayama, H.: Low-velocity projectile impact on spacecraft. Acta Astronaut. **47**(10), 763–770 (2000)

6. Deutschen, N.R., Bowers, E.J., Lankford, J.W.: ASCC: the impact of a silver bullet. AT&T Tech. J. **75**(1), 24–34 (1996)
7. Chang, W.R., Ling, F.F.: Normal impact model of rough surfaces. ASME J. Tribol. **114**, 439–447 (1992)
8. Greenwood, J.A., Williamson, J.B.P.: Contact of nominally flat surfaces. Proc. R. Soc. Lond. A **295**, 300–319 (1966)
9. Bogy, D.B., Stanley, H.M., Donovan, M., Cha, E.: Some critical tribological issues in contact and near-contact recording. Santa Clara, CA (1993)
10. Poon, C.Y., Bhushan, B.: Nano-asperity contact analysis and surface optimization for magnetic head slider/disk contact. Wear **202**(1), 83–98 (1996)
11. Weidong, H., Bogy, D.B., Honchi, M.: An asperity contact model for the slider air bearing. ASME J. Tribol. **122**(2), 436–443 (2000)
12. Green, I.: A transient dynamic analysis of mechanical seals including asperity contact and face deformation. Tribol. Trans. **45**(3), 284–293 (2002)
13. Sochting, S., Sherrington, I., Lewis, S.D., Roberts, E.W.: An evaluation of the effect of simulated launch vibration on the friction performance and lubrication of ball bearings for space applications. Wear **260**(11–12), 1190–1202 (2006)
14. Qiang, Y., Watanabe, K., Tsurusawa, T., Shiratori, M., Kakino, M., Fujiwara, N.: The examination of the drop impact test method. In: The Ninth Intersociety Conf. on Thermal and Thermomechanical Phenomena in Electronic Systems (IEEE Cat. No. 04CH37543), Las Vegas, NV, USA. IEEE Press, New York (2004)
15. Wong, E.H., Lim, C.T., Field, J.E., Tan, V.B.C., Shim, V.P.W., Lim, K.M., Seah, S.K.W.: Tackling the drop impact reliability of electronic packaging. In: ASME International Electronic Packaging Technical Conference and Exhibition, Haui, HI (2003)
16. Marghitu, D.B.: Impact of a planar flexible bar with geometrical discontinuities of the first kind. Phil. Trans. R. Soc. Lond. A **359**, 2595–2608 (2001)
17. Chang, W.R., Etsion, I., Bogy, D.B.: An elastic-plastic model for the contact of rough surfaces. ASME J. Tribol. **109**(2), 257–263 (1987)
18. Jackson, R.L., Green, I.: A finite element study of elastoplastic hemispherical contact. ASME J. Tribol. **127**(2), 343–354 (2005)
19. Yang, J., Komvopoulos, K.: Impact of a rigid sphere on an elastic homogeneous half-space. ASME J. Tribol. **127**(2), 325–330 (2005)
20. Thornton, C.: Coefficient of restitution for collinear collisions of elastic-perfectly plastic spheres. J. Appl. Mech. **64**(2), 383–386 (1997)
21. Wu, C.-Y., Li, L.-Y., Thornton, C.: Energy dissipation during normal impact of elastic and elastic-plastic spheres. Int. J. Impact Eng. **32**(1–4), 593–604 (2005)
22. Li, L.Y., Wu, C.Y., Thornton, C.: A theoretical model for the contact of elastoplastic bodies. Proc. Inst. Mech. Eng., C J. Mech. Eng. Sci. **216**(4), 421–431 (2002)
23. Weir, G., Tallon, S.: The coefficient of restitution for normal incident, low velocity particle impacts. Chem. Eng. Sci. **60**(13), 3637 (2005)
24. Johnson, K.L.: Contact Mechanics. Cambridge University Press, Cambridge (1985)
25. Vu-Quoc, L., Zhang, X.: An elastoplastic contact force-displacement model in the normal direction: displacement-driven version. Proc. R. Soc. Lond. A **455**(1991), 4013–4044 (1999)
26. Timoshenko, S., Goodier, J.N.: Theory of Elasticity. McGraw-Hill, New York (1951)
27. Kogut, L., Etsion, I.: Elastic-plastic contact analysis of a sphere and a rigid flat. ASME J. Appl. Mech. **69**(5), 657–662 (2002)
28. Green, I.: Poisson ratio effects and critical values in spherical and cylindrical Hertzian contacts. Int. J. Appl. Mech. Eng. **10**(3), 451–462 (2005)
29. Quicksall, J.J., Jackson, R.L., Green, I.: Elasto-plastic hemispherical contact models for various mechanical properties. Proc. Inst. Mech. Eng., J J. Eng. Trib. **218**(4), 313–322 (2004)
30. Chaudhri, M.M., Hutchings, I.M., Makin, P.L.: Plastic compression of spheres. Philos. Mag. **49**(4), 493–503 (1984)
31. Johnson, K.L.: An experimental determination of the contact stresses between plastically deformed cylinders and spheres. In: Engineering Plasticity. Cambridge University Press, Cambridge (1968)
32. Zhao, Y., Maletta, D.M., Chang, L.: An asperity microcontact model incorporating the transition from elastic deformation to fully plastic flow. ASME J. Tribol. **122**(1), 86–93 (2000)
33. Wu, C.Y., Li, L.Y., Thornton, C.: Rebound behaviour of spheres for plastic impacts. Int. J. Impact Eng. **28**, 929–946 (2003)
34. Etsion, I., Kligerman, Y., Kadin, Y.: Unloading of an elastic-plastic loaded spherical contact. Int. J. Solids Struct. **42**(13), 3716–3729 (2005)
35. Jackson, R.L., Chusoipin, I., Green, I.: A finite element study of the residual stress and strain formation in spherical contacts. ASME J. Tribol. **127**(3), 484–493 (2005)
36. Kharaz, A.H., Gorham, D.A.: A study of the restitution coefficient in elastic-plastic impact. Philos. Mag. Lett. **80**(8), 549–559 (2000)
37. Shankar, S., Mayuram, M.M.: Effect of strain hardening in elastic-plastic transition behavior in a hemisphere in contact with a rigid flat. Int. J. Solids Struct. **45**(10), 3009–3020 (2008)
38. Jones, N.: Structural Impact. Cambridge University Press, Cambridge (1989)
39. Minamoto, H., Seifried, R., Eberhard, P., Toyoda, J., Kawamura, S.: Influence of strain rate sensitivity on multibody impact. In: Proceedings of the 56th Tokai Branch Regular Meeting of the Japan Society of Mechanical Engineers, **073-1(2007-3)**, pp. 51–52 (2007) (in Japanese)